



# Friction-stir processing of a cold sprayed AA7075 coating layer on the AZ31B substrate: Structural homogeneity, microstructures and hardness



F. Khodabakhshi<sup>a,\*</sup>, B. Marzbanrad<sup>b</sup>, L.H. Shah<sup>b,c</sup>, H. Jahed<sup>b</sup>, A.P. Gerlich<sup>b</sup>

<sup>a</sup> School of Metallurgical and Materials Engineering, College of Engineering, University of Tehran, P.O. Box: 11155-4563, Tehran, Iran

<sup>b</sup> Department of Mechanical and Mechatronics Engineering, University of Waterloo, Waterloo, ON, Canada

<sup>c</sup> Faculty of Mechanical Engineering, Universiti Malaysia Pahang, Pahang, Malaysia

## ARTICLE INFO

**Keywords:**  
Cold gas dynamic spray  
AA7075 coating  
AZ31B substrate  
Friction-stir processing  
Microstructure

## ABSTRACT

In this study, the cold gas dynamic spraying (CGDS) process was employed to modify the surface of AZ31B magnesium alloy with an aluminum-zinc alloy (AA7075). Friction-stir processing (FSP) was subsequently applied as a solid-state localized surface modification technique to improve the structure and integrity of the cold sprayed layer, by enhancing densification, homogeneity, and microstructural features of the as-deposited material. The structure of precipitates and grains were also refined due to the applied severe plastic deformation during FSP, which ultimately affects the indentation hardness resistance of the processed AZ31B-AA7075 bi-metallic structure. Microscopy indicated slight grain coarsening within the AZ31B substrate occurred simultaneously with refinement of the AA7075 coating, along with significant hardness improvements of ~80% and 30% respectively for each region in terms of Vickers hardness after FSP.

## 1. Introduction

Magnesium and its alloys are among the most highly investigated light structural materials which offer high strength to weight ratio, enabling corresponding fuel efficiency through significant weight savings [1]. Therefore, they have recently attracted considerable attention for various transportation applications such as automotive and aerospace, and also consumer electronics industries as well [2]. The most well-known magnesium alloys are AZ series which are alloyed with aluminum (Al) and zinc (Zn) [3]. Among them, AZ31 is one of the most popular commercial magnesium alloys which offer great potential as a replacement for aluminum and steel for a variety of scenarios including aircraft fuselages, engine blocks, cell phone and computer cases, bicycle frame, speaker cones and concrete tools [3]. Despite the unique specific mechanical properties, application of these magnesium alloys has been limited due to poor hardness, wear resistance, and corrosion [4,5]. However, these deficiencies can be offset by other means, such as reinforcing the Mg-metal matrix with ceramic secondary phase nanoparticles to fabricate composites with improved properties [6,7].

One effective way to enhance most properties is to coat the surface of magnesium alloys with another hard corrosion resistant metal or alloy [8,9]. Aluminum alloys offer good potential for surface protection in selected environments and conditions, especially compared to Mg alloys. Among them, AA2xxx and AA7xxx series offer among the

highest mechanical strength and hardness [10], although corrosion resistance is strongly dependent on the chemical composition of the alloy. The corrosion protection offered these alloys is already superior to Mg alloys as coating layer, and a combination of enhanced corrosion resistance and surface hardening can be further realized with additional thermomechanical processing. Meanwhile, selecting the processing technique to prepare this magnesium-aluminum bi-metallic structure is rather critical due to their sensitivity to temperature [11,12]. Also the coating of complex shapes like an engine block for instance is not possible using common cladding technologies such as roll bonding or pressing [13].

Cold gas dynamic spray (CGDS) is a material deposition process which can be used for the aim of surface modification, which involves high velocity ballistic impact of metallic or non-metallic particles on the surface of a metallic substrate [14]. Using this cold spray technology it is possible to deposit a wide range of coating thicknesses by controlling the characteristics of the feeding powder and metal substrate, gas temperature, gas pressure, powder feeding rate, nozzle geometry, and gun traverse velocity [15–17]. This process has been recently employed for surface modification in various aircraft and automobile structural applications in the transportation industries [18]. As a result of high strain rate impingement of particles, a wavy mechanical inter-locking interface along with metallurgical bonding forms between the coating and substrate materials [15,19].

\* Corresponding author.

E-mail addresses: [farzadkhodabakhshi83@gmail.com](mailto:farzadkhodabakhshi83@gmail.com), [fkhodaba@uwaterloo.ca](mailto:fkhodaba@uwaterloo.ca) (F. Khodabakhshi).

The high velocity interaction between the feeding particles and substrate leads to the generation of primary bonding according to the “adiabatic shear instability” mechanism [20–22]. In this process, the temperature rise caused by the gas stream along with ‘jetting’ of the material at the particle interfaces during impact can accelerate the formation of metallurgical bonding [17]. However, excessive pre-heating of the carrier gas can melt the feeding particles or metal substrate, which should be avoided to prevent microstructural changes and undesirable phase transformations [15]. Since the impacting materials remain in the solid state, the surface metal-matrix composite or bi-metallic coatings offer unique characteristics in many regards [14,23]. This has led to a broad range of research using this process for production and modification of different metallic and non-metallic systems [23–25], although there are limited reports about optimizing the CGDS processing parameters to create aluminum coatings on magnesium substrates for modification [26–34]. In the present research, CGDS was employed using optimized processing parameters to deposit a uniform layer of aluminum-zinc alloy (AA7075) on the surface of AZ31B magnesium alloy sheet. The microstructural features and mechanical properties of the produced AZ31B-AA7075 bi-metallic structure were studied using a combination of metallographic techniques and hardness testing.

During the CGDS process, gas trapped between the particles during deposition process can make the coating porous, leading to a degradation of mechanical properties of the coating and its bond to the substrate [14,17]. Under mechanical loading during service and especially in the cyclic condition, this coating layer can easily delaminate and with exposure to corrosive media, which can lead to intensified local corrosion which quickly deteriorates the structure [11,12,28]. Therefore, in this study a new post modification technique is introduced to compliment the cold spray process and enhance the adhesion, structural homogeneity and promote densification of the coated aluminum layer, leading to stronger metallurgical bonding with the magnesium substrate. This investigation is also highly relevant to the manufacturing of bulk metals and alloys by additive cold spraying which have also recently attracted strong interest [35,36].

Friction-stir processing (FSP) as a new and very effective solid-state surface modification technique, which was first reported by Mishra et al. [37,38] as method for producing ultra-fine grain structures that exhibits superplasticity [39], homogenization the structure of powder metallurgy and cast materials [40], and also generates the *ex situ* and *in situ* metal-matrix surface nanocomposites [41–44]. In this method, a non-consumable rotating tool with a specially designed shoulder and pin is plunged into the surface of metal to be modified and then moved along the direction of interest [45]. The localized frictional heating between the rotating tool and workpiece leads to materials softening around the pin and by materials extrusion during a complex flow from advancing side toward the retreating side of the processed or stirred zone is formed at solid-state [38,46]. Therefore, FSP offers great potential for homogenizing and microstructural modification of powder metallurgy processed alloys/composites, and can be used to eliminate casting defects, while also breaking up or dissolves the secondary phase particles (leading to considerable improvement in the mechanical properties), and can also be used for fabrication of surface metal-matrix composites [47–49].

There are only few reports in the literature about the modification of CGDS coatings by friction-stir processing (FSP) [50–55]. In the first work by Hodder et al. [50], Al-Al<sub>2</sub>O<sub>3</sub> metal-matrix composite coatings were deposited with extremely high contents of reinforcing agent (> 90 wt%) on the surface of an AA6061 aluminum alloy and modified by FSP, leading to a considerable improvement in hardness. Ashrafizadeh et al. [52], also demonstrated the benefit of FSP on the wear rate of cold spray deposited tungsten carbide-based metal matrix composites on the surface of low carbon steel substrate. The main finding indicated a considerable improvement in abrasive wear resistance of the modified coatings after FSP in comparison to the as-sprayed coatings. As reported

**Table 1**  
Chemical composition of the utilized AZ31 magnesium alloy substrate (wt%).

Element	Mg	Al	Zn	Mn	Fe	Ni	Si	Cu
AZ31 alloy	Base	2.92	1.09	0.3	0.005	0.005	0.01	0.05

**Table 2**  
Chemical composition of the used AA7075 coating powders (wt%).

Element	Al	Zn	Mg	Cu	Fe	Cr	Others
AA7075 particle	Base	5.2	2.35	1.55	0.35	0.25	0.3

**Table 3**  
The employed parameters and conditions for cold gas dynamic spraying process.

Processing equipments and conditions		Type and value
Carrier gas		Nitrogen
Gas pressure		1.4 MPa (200 psi)
Gas temperature		400 °C
Feeding rate		5 rpm (8 g/min)
Traverse velocity		2 mm/s
Step over		1.2 mm
Stand-off distance		12 mm
Nozzle type		De Laval Ulti-Life TM
Nozzle length		120 mm
Nozzle orifice diameter		2 mm
Nozzle exit diameter		6.3 mm

**Table 4**  
Specifications of the utilized FSP tool.

Shoulder diameter	Concave shoulder angle	Pin diameter	Pin height
12 mm	3°	1.7 mm	1.5 mm

by Peat et al. [53], the erosion performance of different WC-CoCr, Cr<sub>3</sub>C<sub>2</sub>-NiCr and Al<sub>2</sub>O<sub>3</sub> metal-matrix composite coatings on the AA5083 substrate was significantly improved by the subsequent implementation of FSP modification technique attributed to the superior uniform distribution of reinforcing particles. Recent work by Huang et al. [54,55], revealed the enhancement in mechanical properties of cold sprayed AA5056-SiC composite coating after structural refinement by FSP. Other work by Huang et al. [51], showed that CGDS and FSP are two emerging and effective solid-state surface modification techniques, which can produce an ultra-fine grained Cu-Zn alloy with enhanced mechanical strength.

In the present work, FSP was applied to a coating deposited by CGDS to provide the following functions; (i) severe plastic deformation to promote mixing and refining of the constituent phases in the cold sprayed bi-materials structure, (ii) elevated temperature deformation to facilitate the formation of intermetallic phases and chemical bonding at the interface, and (iii) hot consolidation to form a fully dense solid coating layer after cold spraying. Therefore, it is expected that this modified cold sprayed bi-metallic AZ31B-AA7075 structure after FSP can exhibit improved hardness. Evolution in the structural features and hardness of cold sprayed material before and after the FSP process were assessed and compared using optical microscopy (OM) observations, field emission-scanning electron microscopy (FE-SEM) analysis, and indentation hardness measurements.

## 2. Experimental procedure

### 2.1. Powder and substrate

In this research, a commercial rolled sheet AZ31B magnesium alloy

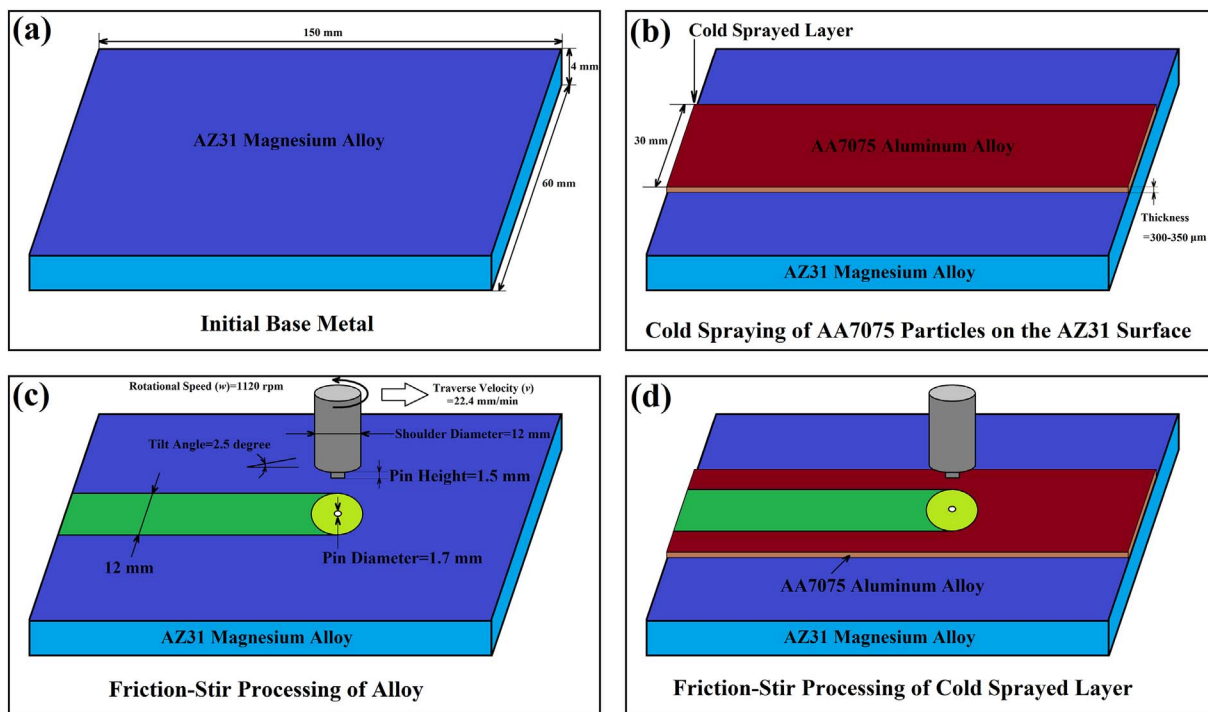


**Fig. 1.** Schematic representations of the (a) initial AZ31B alloy substrate, (b) cold spraying of an AA7075 layer on the AZ31B substrate, (c) FSP of initial AZ31B alloy, and (d) FSP of the cold sprayed AZ31B-AA7075 bi-materials structure.

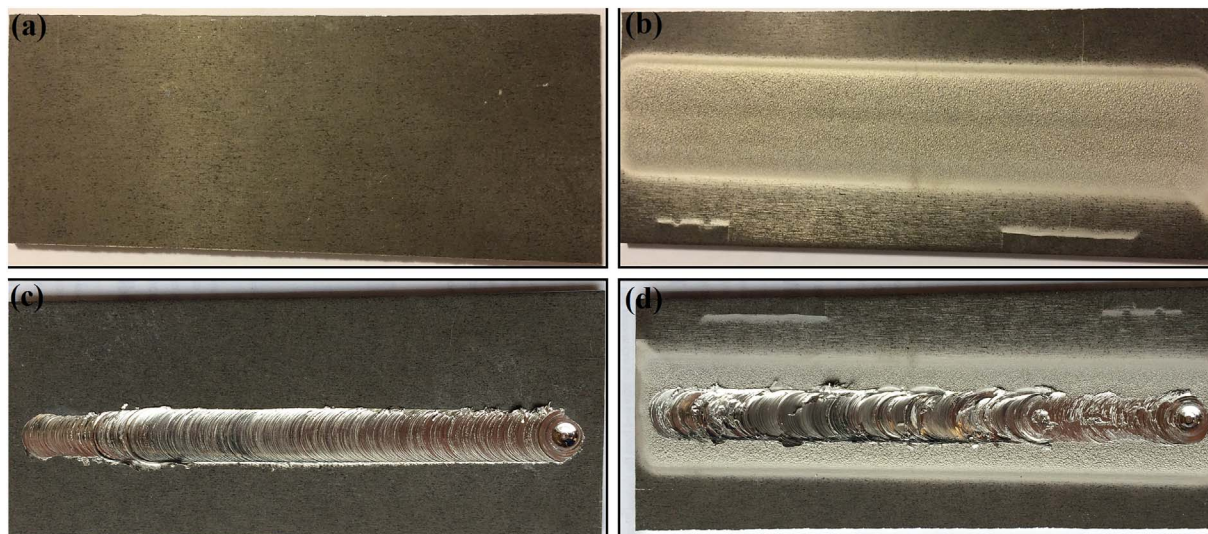


**Fig. 2.** Experimentally prepared samples for the previous images; (a) initial AZ31B alloy substrate, (b) cold spraying of an AA7075 layer on the AZ31B substrate, (c) FSP of initial AZ31B alloy, and (d) FSP of the cold sprayed AZ31B-AA7075 bi-materials structure.

with a thickness of 4 mm and chemical composition as shown in Table 1 was used as the substrate. This alloy was used in the H24 initial temper condition. The sheet of this alloy was cut into the small samples with dimensions of 150 mm × 60 mm along the rolling direction, before coating by CGDS process. Moreover, the AA7075 (aluminum-zinc alloy) powders with an average particle size of 23  $\mu\text{m}$  were purchased from the Center-line Company (Centerline Co., Windsor, Ontario, Canada) and used as the coating material with the composition as reported in Table 2.

## 2.2. Cold gas dynamic spraying

In this study, the cold gas dynamic spraying (CGDS) process was employed to produce a coating from AA7075 alloy on the AZ31B

substrate. Electronic Supporting Information (ESI) Fig. S1 shows the SST model P low pressure cold spray system manufactured by the Center-line Company (Centerline Co., Windsor, Ontario, Canada) used for the coating of the AA7075. The processing parameters for deposition are summarized in Table 3. For cold spray deposition, gas pressure, powder feeding rate and nozzle traverse velocity as the main parameters were varied in the ranges of 180–220 psi, 4–10 rpm, and 1–4 mm/s, respectively and optimized to make a coating with acceptable appearance and sufficient thickness for processing as reported in Table 3.

## 2.3. Friction-stir processing

To enhance the structural characteristics of the deposited cold

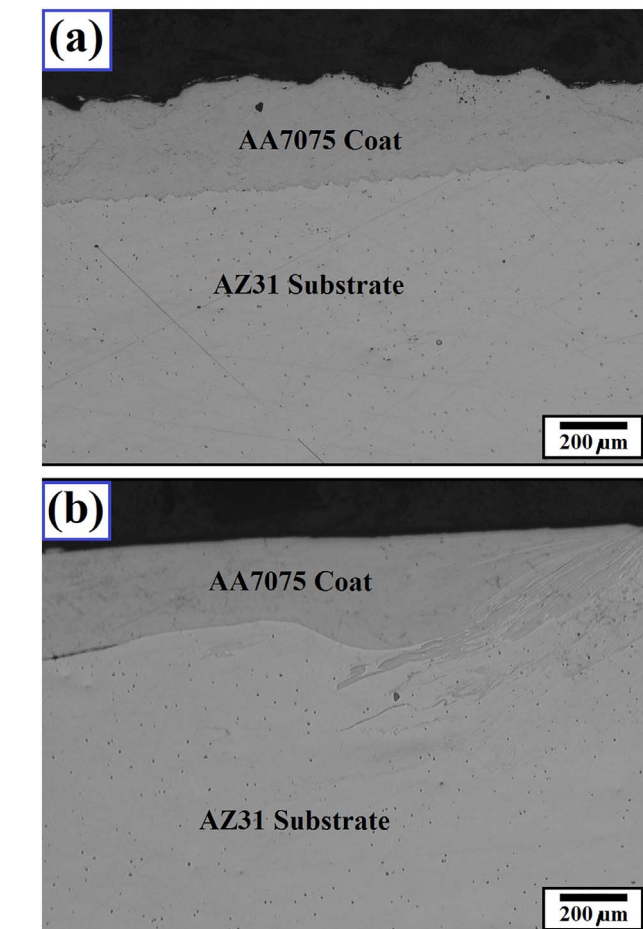
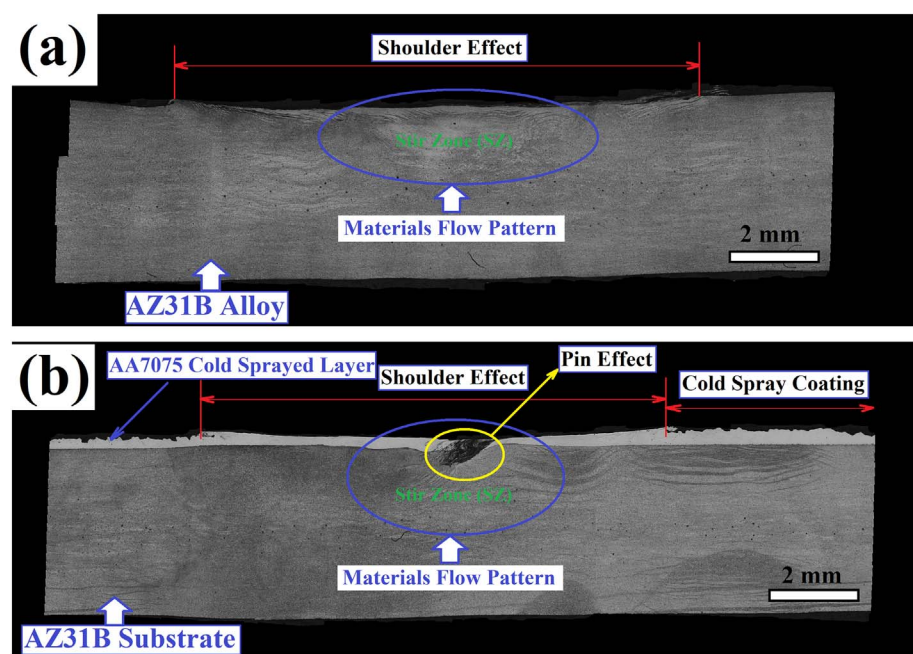


**Fig. 4.** Optical micro-graphs from the materials inter-mixing flow patterns for the cold sprayed layer (a, b) before and (c, d) after FSP process.

sprayed layer, friction-stir processing (FSP) was employed as a secondary method. For this purpose, a high torque and displacement controlled 7.5 HP spindle vertical milling machine (Jafco Universal Milling Machine, Jarocin, Poland) as shown in ESI Fig. S2a was used.

**Fig. 3.** Macro-images made by combining the optical micro-images from the thickness cross-sections of the FSPed (a) AZ31B alloy, and (b) cold sprayed AZ31B-AA7075 bi-materials structure.

During post deposition modification by FSP, it is critical to avoid the material vertical flow (through the thickness direction) which can lead to magnesium being displaced to the top surface through the coating. Since, this material flow is mainly controlled by the pin length and diameter, and the presence of pin threads [56]; therefore it would be useful to keep these dimensions as small as possible. Thus, using a cylindrical smooth tool without threads would suppress intermixing material flow. As a result, a specialized tool geometry was made from H13 steel and employed in comparison to those commonly used in friction-stir joining technologies. The particular design for this simple cylindrical tool is illustrated in ESI Fig. S2b, with the main specifications as expressed in Table 4. FSP parameters were employed to minimize the machine vibrations in order to perform the process in a stable condition, in which a rotational speed ( $w$ ) of 1120 rpm and a traverse velocity ( $v$ ) of 22.4 mm/min were applied. Actually, these parameters related to the FSP variables were varied in the ranges of 600–1200 rpm and 12.5–60 mm/min, respectively and optimized in advance, in order to achieve a sound and effective friction-stir processing condition on the coating layer. Also, the tilt angle was kept constant at about 2.5° during processing. One FSP pass with these conditions was performed on the cold sprayed sample along the rolling direction. For the purpose of comparison, the AZ31B alloy without coating was friction stir processed at the same conditions as well. Therefore, as shown in the schematic representations of Fig. 1 and real images of Fig. 2, four samples were produced and considered for further investigations, including: (i) initial AZ31B alloy (Figs. 1a and 2a), (ii) cold sprayed AZ31B-AA7075 bi-material sample (Figs. 1b and 2b), (iii) FSPed AZ31B alloy (Figs. 1c and 2c), and (iv) FSPed cold sprayed AZ31B-AA7075 bi-material sample (Figs. 1d and 2d).

#### 2.4. Microstructure

These processed samples were cross-sectioned perpendicular to the rolling or FSP directions for the aim of microstructural investigations across the thickness section. After standard metallographic preparation procedures, including mechanical grinding up to the #3000 grade number and polishing using 0.1 μm diamond paste, etching was performed using a reagent composed of 5 mL water, 35 mL ethanol, 5 mL acetic acid, and 2.1 g picric acid, which was employed for about 10 s to reveal the grain structure of AZ31B magnesium alloy before and after FSP. Also, the grain structure of the AA7075 coating was revealed using

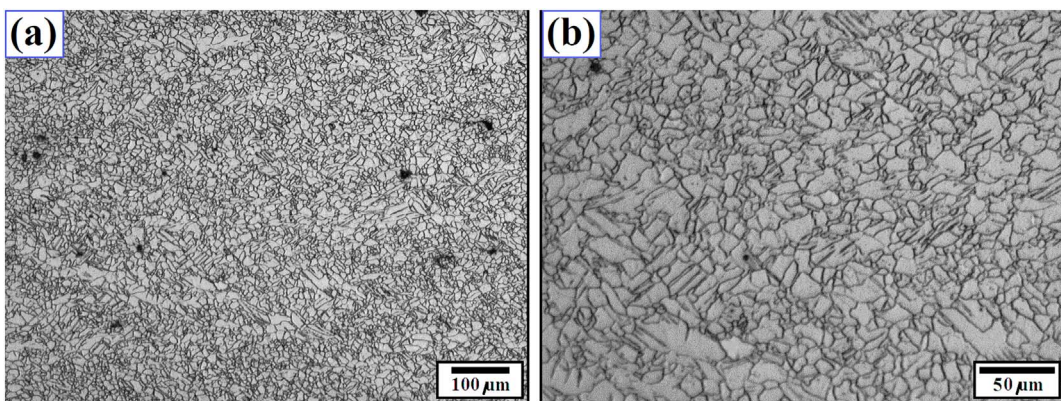


Fig. 5. Optical micro-graphs showing the grain structure of initial AZ31B alloy from different regions at different magnifications.

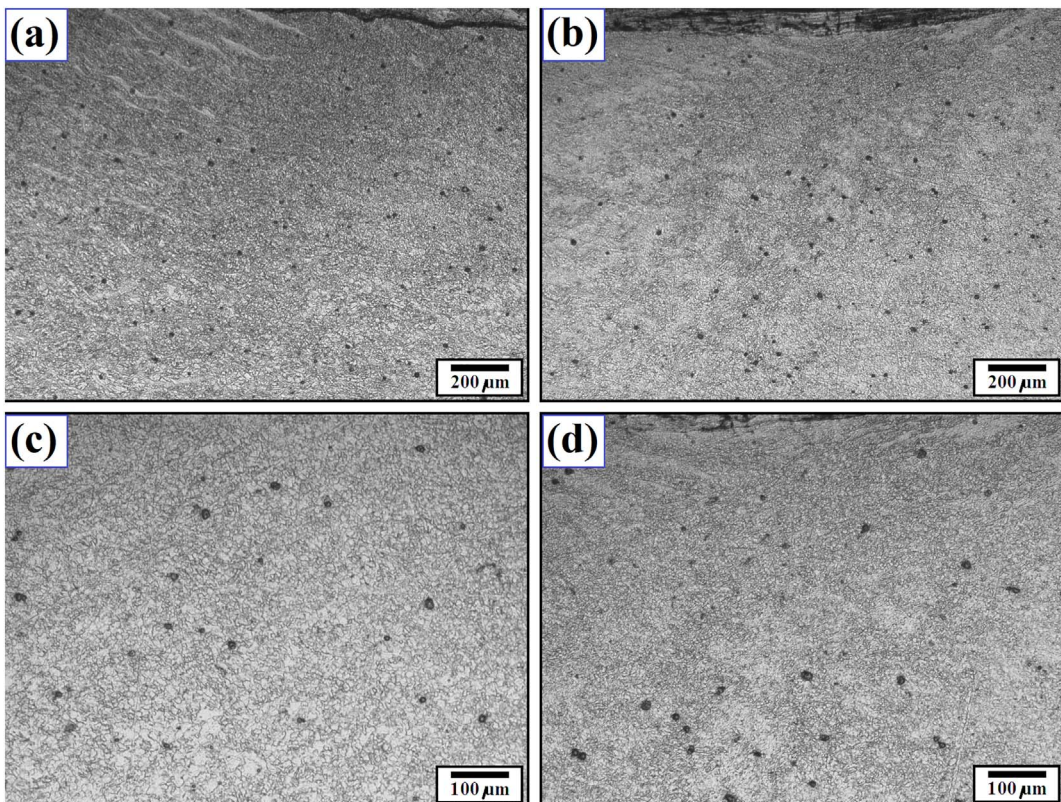


Fig. 6. Optical micro-graphs showing the grain structure of FSPed AZ31B alloy within the SZ at different magnifications.

Keller's reagent ( $190\text{ mL H}_2\text{O} + 5\text{ mL HNO}_3 + 3\text{ mL HCl} + 2\text{ mL HF}$ ) for about a 15 s holding time. Microstructures of the prepared samples at different regions, *i.e.*, the base metal (BM), heat affected zone (HAZ), thermo-mechanical affected zone (TMAZ), and stir zone (SZ), were studied by using stereographic (Nikon, USA), optical (OM, Olympus PME3, Germany), and field emission-scanning electron microscopy (FE-SEM, JEOL 7600, Japan) analyses. This FE-SEM microscope operated with an acceleration voltage of 50 keV, a beam current of 40 mA, while equipped with an energy-dispersive X-ray spectroscopy (EDS) detector as well to perform the chemical analysis.

## 2.5. Hardness testing

To assess the mechanical durability of the AZ31B alloy and cold sprayed AZ31B-AA7075 bi-material sample before and after employing the FSP process, indentation hardness of different regions was evaluated. A NANOVEA M1 Hardness Indenter (NANOVEA, USA) was used

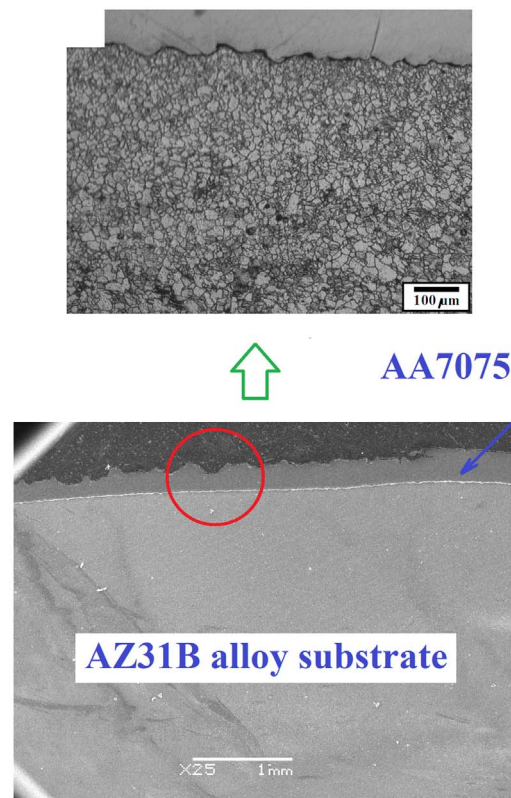
to perform the indents. In this machine, main parameters were set as approach load of 10  $\mu\text{m}/\text{min}$ , contact load of 15 mN, applied load of 5 N, loading rate of 10 N/min, unloading rate of 10 N/min, and holding time of 5 s. In addition to the Vickers hardness values, load-depth graphs during indentation testing were monitored and reported. To check the repeatability of data and also the hardness profiles, for each region the measurements were carried out at least three times.

## 3. Results and discussion

### 3.1. Materials flow pattern and microstructural evolutions during cold spraying and FSP processes

The cross-sections which reveal the material flow patterns from the initial AZ31 alloy and cold sprayed AZ31-AA7075 bi-metallic structure after FSP process are shown in the stereographic images of Fig. 3a and b, respectively. Since the pin diameter of the FSP tool was designed to

### Grain structure of substrate after cold spray



### Grain structure of cold spray layer

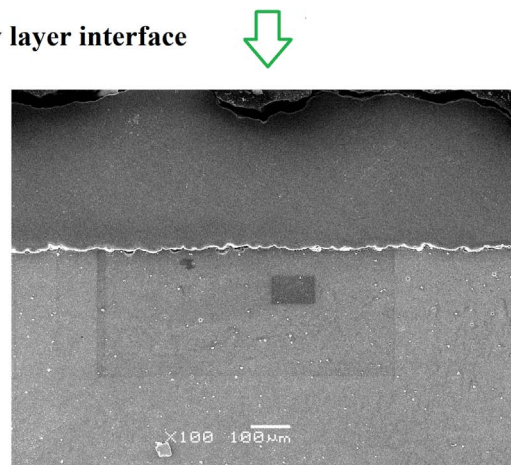
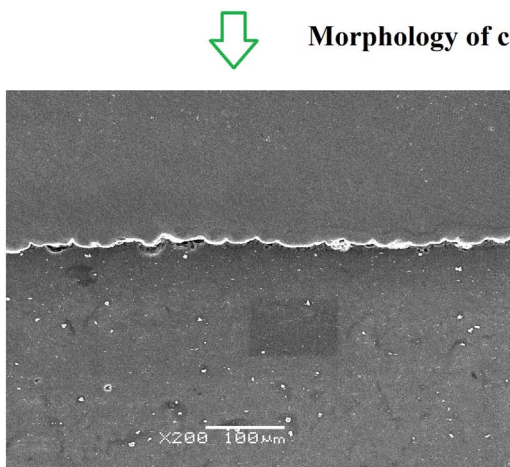
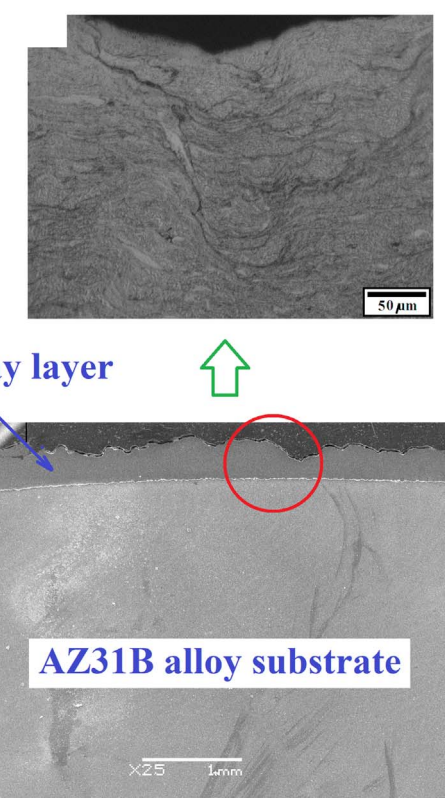


**Fig. 7.** Macro-images, grain structures and interface morphology for the AA7075 coating layer and AZ31B alloy substrate after cold spray deposition.

be rather small, most of the structural refinement occurred close to the surface in contact with the tool shoulder, and only a small SZ volume formed. After etching, the optical microstructures across the thickness section of the cold sprayed coated layer on the magnesium substrate before and after FSP are compared in Fig. 4a and b, respectively. It can be noted the final thickness of deposited material in the as-sprayed sample is in the range of 200–250  $\mu\text{m}$ , and that the surface roughness of the cold spray deposited layer is eliminated after the FSP process resulting in a smooth and flat coating. Also, the interface between the AA7075 coating and AZ31B substrate changed from a wavy to a smoother profile. A small crack-like feature at the substrate-coating interface can be seen in Fig. 4b (left side) which is located at the re-treating side and close to the pin-side effect. Also, the texture profile in Fig. 4b is due to materials mixing by the influence of small pin. However, further detailed study is necessary to characterize the boundary of

coated layer.

The optical grain structure of the initial AZ31B magnesium alloy is shown in Fig. 5. Since this alloy was in the H24 temper condition, its microstructure can be characterized as a cast that was homogenized before rolling, which involved the formation of magnesium dendrites with an Al-rich solid-solution with interdendritic  $\beta\text{-Mg}_{17}\text{Al}_{12}$  intermetallic phase [3]. Considering the processing technology employed, some slightly different grain structures can be observed at the center of the processed zone compared to the surface edge when studying the as-received magnesium sheet. As shown in Fig. 6, after FSP the grain structure in the SZ is significantly refined and becomes mostly equiaxed. An average grain size of  $< 5 \mu\text{m}$  can be noted, while the as-received grain structure of the magnesium substrate was in the range of 10–15  $\mu\text{m}$ .

It is well known that frictional heating generated in the SZ during

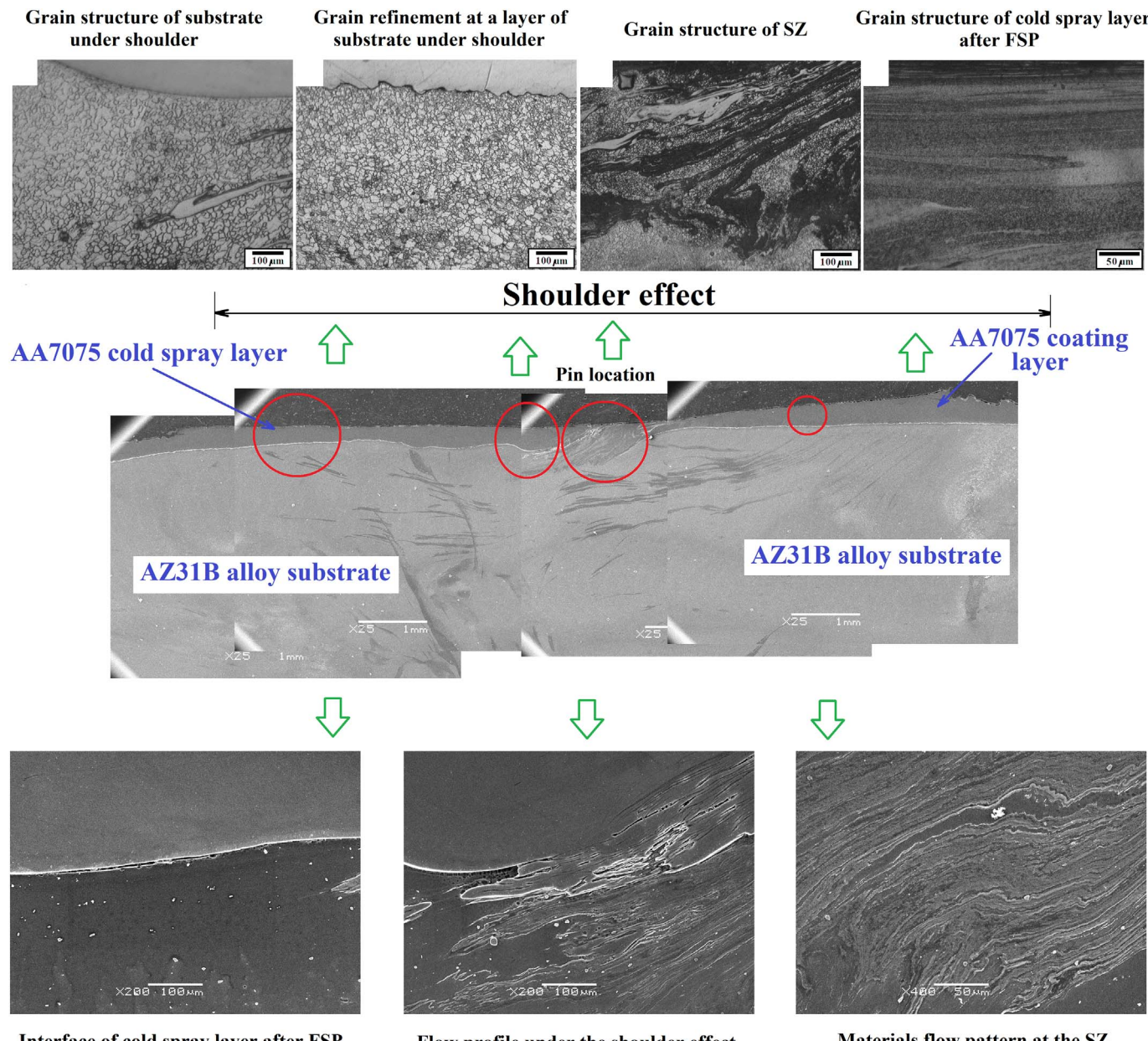


**Fig. 8.** A combined image from the optical and FE-SEM micro-graphs showing the flow pattern, materials mixing and grain structure of different regions for the cold sprayed sample after FSP modification.

FSP along with intense plastic deformation at high temperatures as caused by the rotating tool leads to significant grain structural refinement through dynamic recrystallization (DRX) mechanism [57]. Although there is a large debate among researchers about the dominant operative dynamic restoration mechanisms during FSP, and how this is influenced by the chemical composition and structure of base material and processing conditions [58]. Figs. 7 and 8 show the flow pattern, material mixing and grain structure corresponding to the different locations of cold sprayed bi-metallic sample before and after FSP modification, respectively. The grain structure of the AZ31B magnesium alloy substrate after cold spray deposition of the AA7075 layer is presented in ESI Fig. S3 with more details as well, and it is clear that the substrate near to the interface is refined after coating. This can be attributed to the high velocity impingement of the aluminum particles impacting the surface at high temperature [19]. However one should also consider the low impact exposure time of 100 to 200 ns during cold spray process, which only facilitates partial recrystallization

phenomenon [59].

In the ESI Fig. S4, microstructures of the substrate at different regions under the shoulder action are revealed after employing FSP modification on the cold sprayed coating. Based on the grain size variation, it seems that grain growth occurred in some regions of the substrate under the coating layer after FSP was applied (see Figs. 7 and 8). Frictional heating between the tool shoulder and contacting work piece surface can accumulate onto the previous cold spray history which leads to continuing the occurrence of DRX up to this stage of grain growth. Around the small rotating pin, high temperatures and materials mixing caused by the intense shear plastic deformation results in significant grain refinement as shown in the optical micro-graphs of Fig. 9. Microstructural features for the cold sprayed AA7075 layer before and after FSP are presented in the optical micro-graphs of Figs. 7 and 8 (see ESI Figs. S5 and S6, as well). Generally, these images indicate the material flow patterns produced by the CGDS process and subsequent FSP modification; however within these flow patterns grain

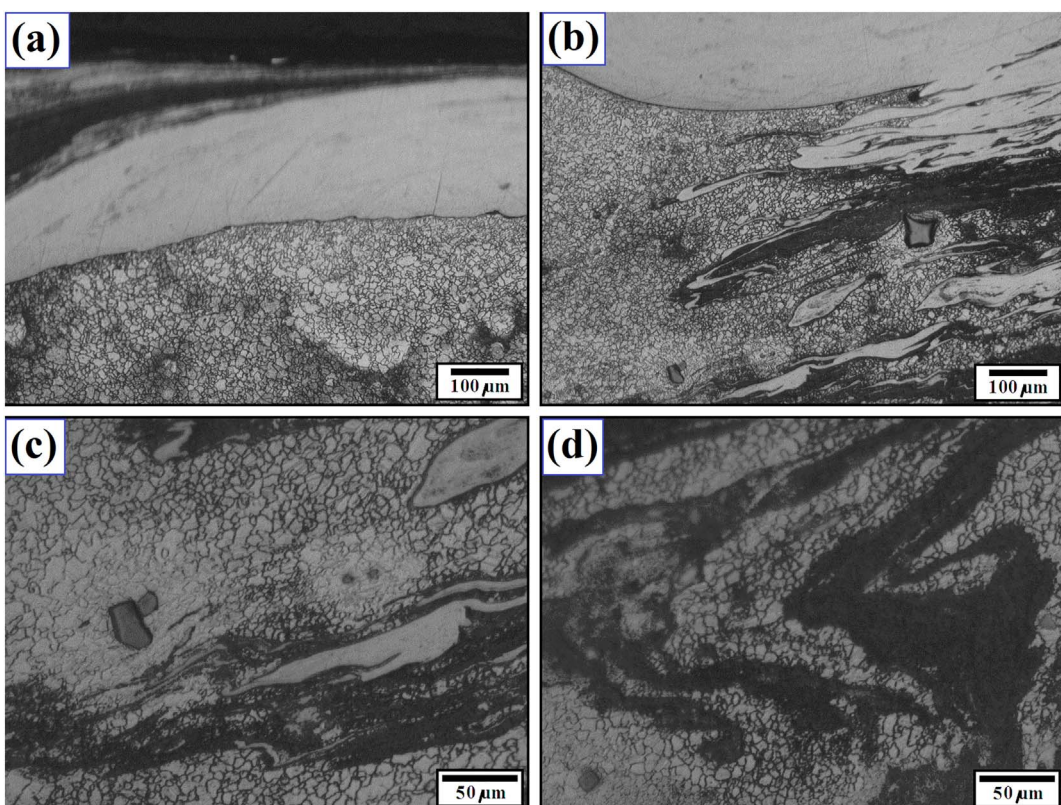


**Fig. 9.** Optical micro-graphs showing the flow pattern and grain structure of FSPed cold sprayed AZ31B-AA7075 sample within the SZ around the rotating small pin at different magnifications.

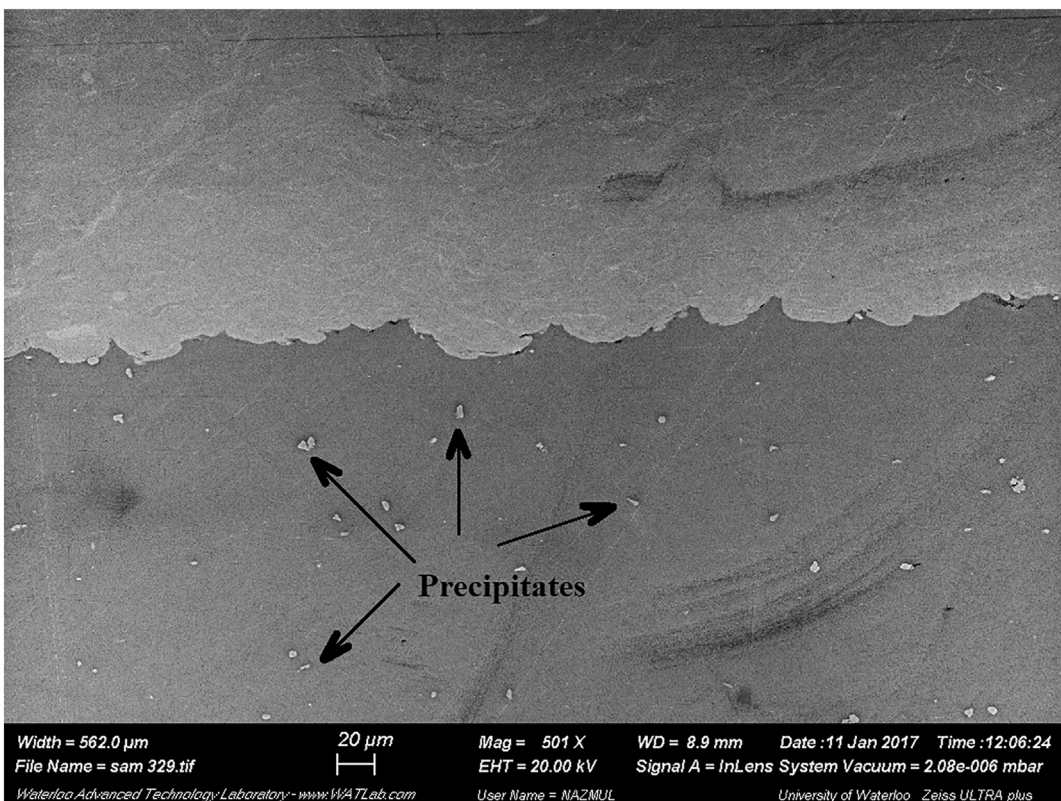


**Fig. 10.** Interface between the AA7075 layer and AZ31B alloy substrate after cold spraying process.

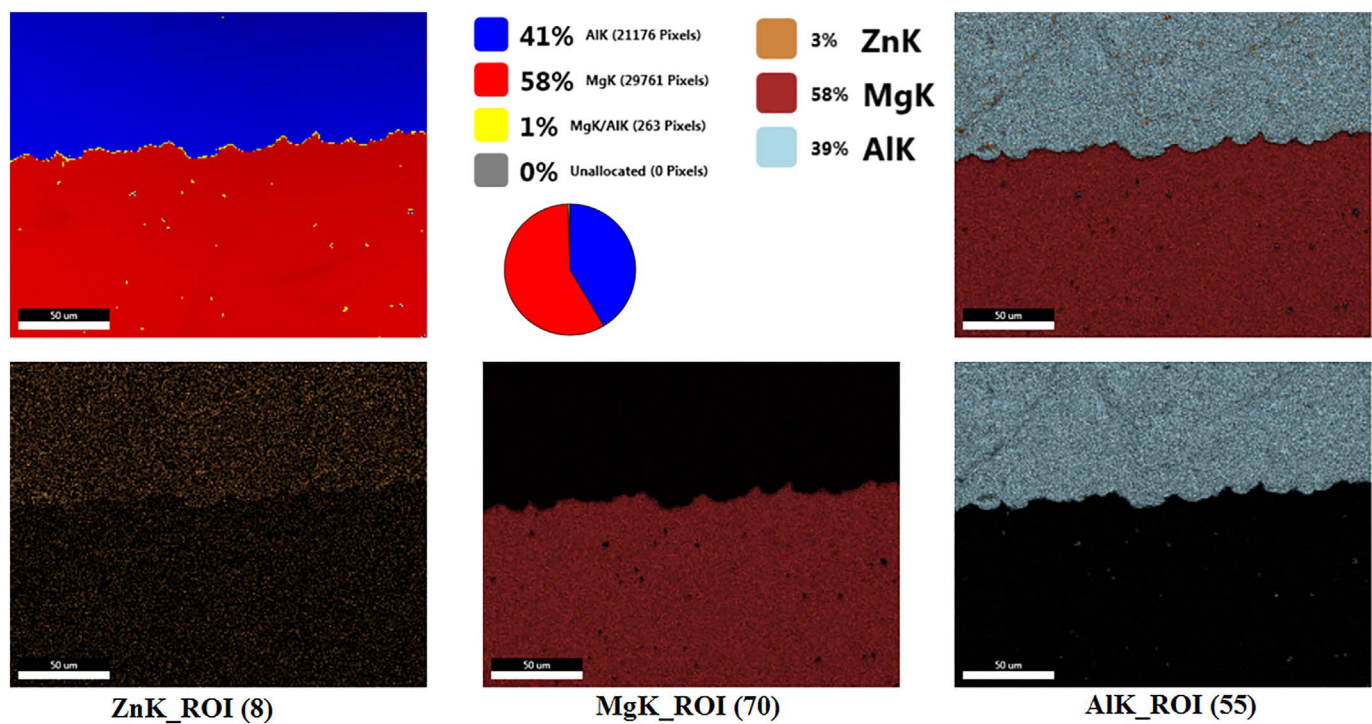


Fig. 11. EDS elemental mapping analysis results from the cold sprayed AZ31B-AA7075 interface.

Fig. 12. Cold sprayed AZ31B-AA7075 interface after FSP modification.



structures are visible as well. For instance, in ESI Fig. S6 l it can be observed that after FSP the mean grain size of AA7075 coating is refined lower than 2  $\mu\text{m}$ . These microstructural developments within the magnesium substrate and aluminum coating during the CGDS and FSP processes affect the mechanical performance of the overall AZ31B-AA7075 bi-metallic structure as examined in the next following sections.

### 3.2. Characterization of microstructural features at the cold sprayed AZ31B-AA7075 interface after FSP modification

FE-SEM images and optical microstructures from the thickness cross-section of the cold sprayed AZ31B-AA7075 sample at different regions are displayed in Fig. 7 (see ESI Fig. S7). High magnification

images from the magnesium/aluminum interface are show in Fig. 7, as well (see ESI Fig. S8). A wavy interface can be observed, and is attributed to the peening effect associated with the high velocity impact of aluminum particles on the substrate surface, as a result of the shear instability which occurs in the CGDS process [15,17]. This kind of wavy interface morphology can improve the bonding strength between the coating layer and substrate due to a more effective mechanical interlocking and improved metallurgical bonding by increasing the contact surface area. Also, the grain structure of substrate under the coated layer was refined as a result of high strain rate plastic deformation and concurrent dynamic recrystallization. The FE-SEM micrographs from the cold sprayed layer cross-sections after FSP modification are shown for different regions in Fig. 8 (for further details see ESI Fig. S9). It was

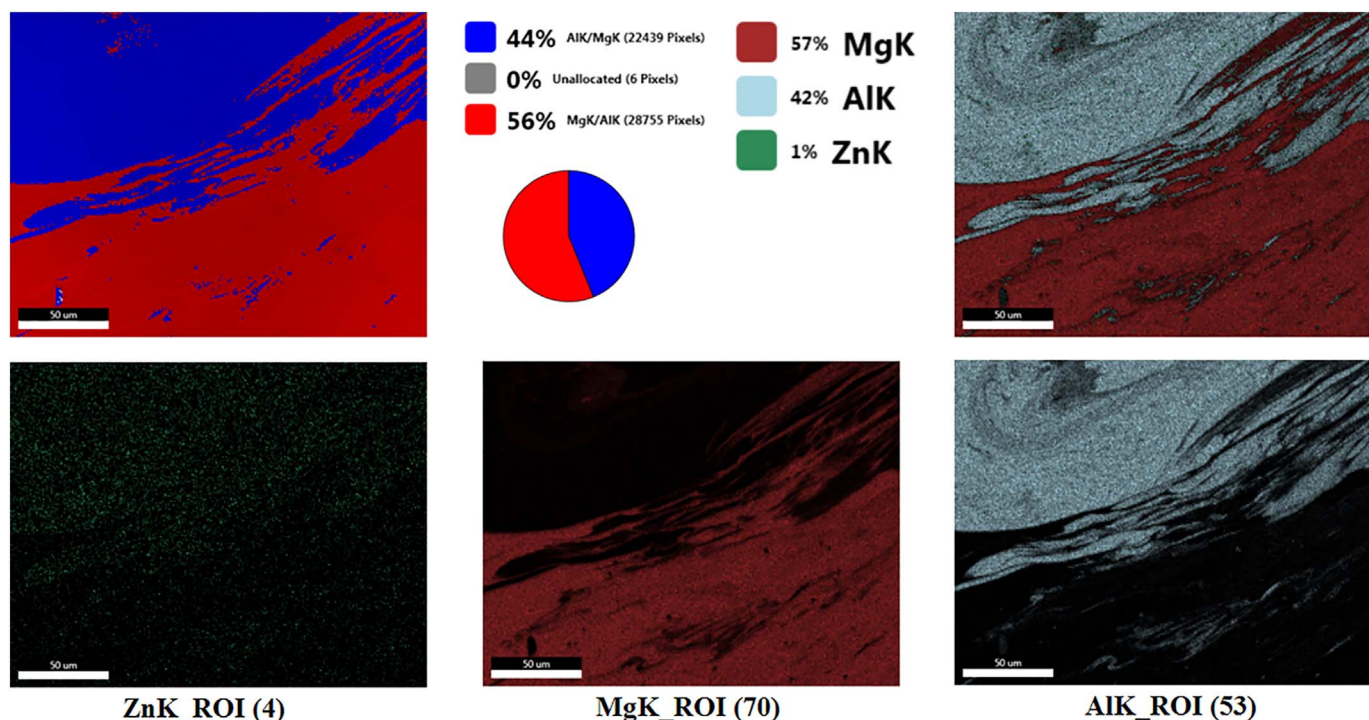


Fig. 13. EDS elemental mapping analysis results from the FSPed cold sprayed AZ31B-AA7075 interface.

found that the deposited aluminum layer becomes denser as a result of the shoulder deformation and thickness reduction (as a rough estimate and without any quantitative measurement). Fig. 8 shows the FE-SEM images from the cold sprayed aluminum-magnesium interface after FSP under the shoulder influence, as well (see ESI Fig. S10). Similar to the optical micro-graphs in Fig. 3, it can be found that the density of the deposited aluminum layer is increased due to the high temperature forging action during FSP, leaving the surface of coated layer completely flat. Moreover, it seems that the wavy pattern at the cold sprayed interface disappeared after FSP modification, likely due to the surface strains imposed.

FE-SEM images of the structural features in the SZ formed by the small pin are presented in Fig. 8 as well, which indicate fine-scale intermixing and some intermingled layers of the aluminum coating layer mixed with the magnesium substrate in this small region, which enables formation of new phases which exhibit white contrast (for further details see ESI Fig. S11). The related features for these new phases can be also found in Figs. 9 and 10, as well. Material flow patterns within the SZ at different magnification are shown in FE-SEM images of Fig. 8 (see ESI Fig. S12), where white flow lines demonstrate the aluminum mixing pattern within the magnesium matrix. Also, white particles within the matrix are attributing to the most favorable intermetallic phase between the aluminum and magnesium elements, i.e., b-Mg<sub>17</sub>Al<sub>12</sub> precipitates. As shown in ESI Fig. 12i, a high fraction of these secondary phase particles which formed at a nano-scale via materials mixing and high temperature severe plastic deformation induced by the FSP process.

FE-SEM images from the cold sprayed AZ31B/AA7075 interface after FSP modification are shown at different magnifications in a region under the shoulder and close to the SZ in Fig. 8 (for further details see ESI Figs. S13a to S13i). However, metallurgical bonding at the interface is maintained and it can be observed that the grain structure of the magnesium substrate is refined down to the ultra-fine (< 1 μm) range close to the interface, assisted by the plastic constraining effect of the high strength aluminum interlocks [47,60] (see ESI Figs. S13 g,h). A high quality FE-SEM image from the wavy interface between the AZ31B substrate and AA7075 coating is shown in Fig. 10.

The EDS elemental analysis maps from distribution of Al, Mg, and Zn elements within the selected region are presented in Fig. 11. Since no inter-diffusion is expected during the CGDS process due to the short impact exposure time there is no overlapping of elements at the interface of the coating. The FE-SEM image and EDS elemental mapping analysis results for this interface after FSP modification are shown in Figs. 12 and 13, respectively. It is clear that the majority of interfaces are not sharp, and some evidence of diffusion is observed based on the presence of elements between the coating and substrate after frictional heating and plastic deformation which promoted material intermixing. Therefore, when employing FSP after the cold spray process the metallurgical bonding between the AZ31B substrate and AA7075 coating improves by a combination of mechanical mixing and inter-diffusion which promotes formation of a thin intermetallic phase.

### 3.3. Indentation testing before and after CGDS and FSP processes

The indentation Vickers micro-hardness tests were performed at different regions of the initial AZ31B magnesium alloy, FSPed alloy, and cold sprayed bi-metallic sample before and after FSP modification, as the results are presented in the optical micrographs of Fig. 14. Also, the corresponding load-depth curves for these measurements are compared in Fig. 15 (see the ESI Figs. S14a to S14f, as well). In these graphs, higher indentation depth under a constant load indicates a lower hardness. The as-received AZ31B-H24 temper magnesium alloy exhibits a mean Vickers hardness number of around 74 HV<sub>0.5</sub> (Fig. 14a). After processing of this alloy, its hardness is considerably increased and varies with location at the stirred zone in relation to the microstructural refinements as reported in Fig. 6. A maximum improvement of about 135 HV<sub>0.5</sub> is attained in the substrate after FSP of AZ31 magnesium alloy, which represents an 80% increase in hardness due to the grained structural refinement (see Fig. 14b). After cold spraying, the hardness of the magnesium substrate close to the interface is enhanced as well due to high impact velocity and subsequent grain refinement as shown in Fig. 9. A maximum hardness enhancement of up to ~40% can be noted in this regard (Fig. 14c). After cold spray deposition of AA7075 particles on the AZ31B substrate, the hardness of the surface is thereby

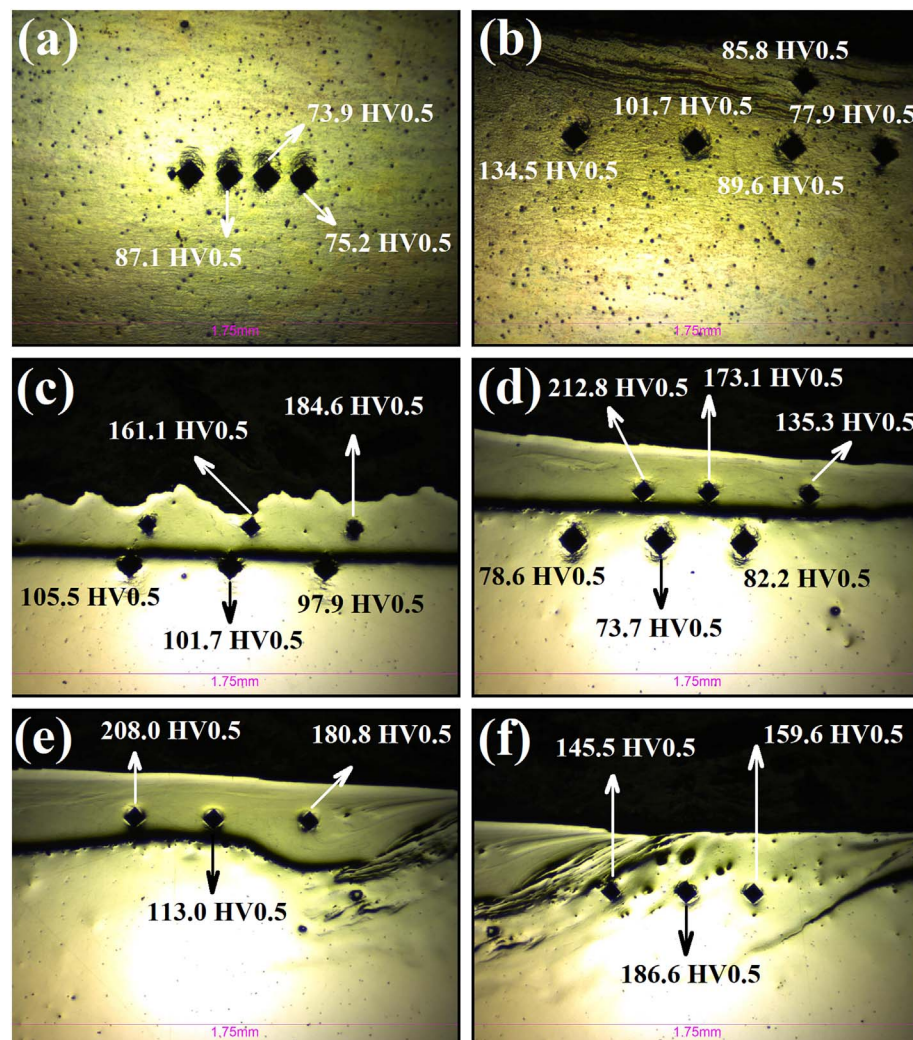


**Fig. 14.** Macro-images showing the micro-hardness profiles across the different regions of FSPed AZ31B alloy and cold sprayed AZ31B-AA7075 bi-metallic samples; (a) initial AZ31B alloy, (b) SZ of FSPed alloy, (c) as-deposited layer, (d) cold sprayed layer after FSP under the shoulder, (e) cold sprayed layer around the small pin, and (f) mixed region at SZ.

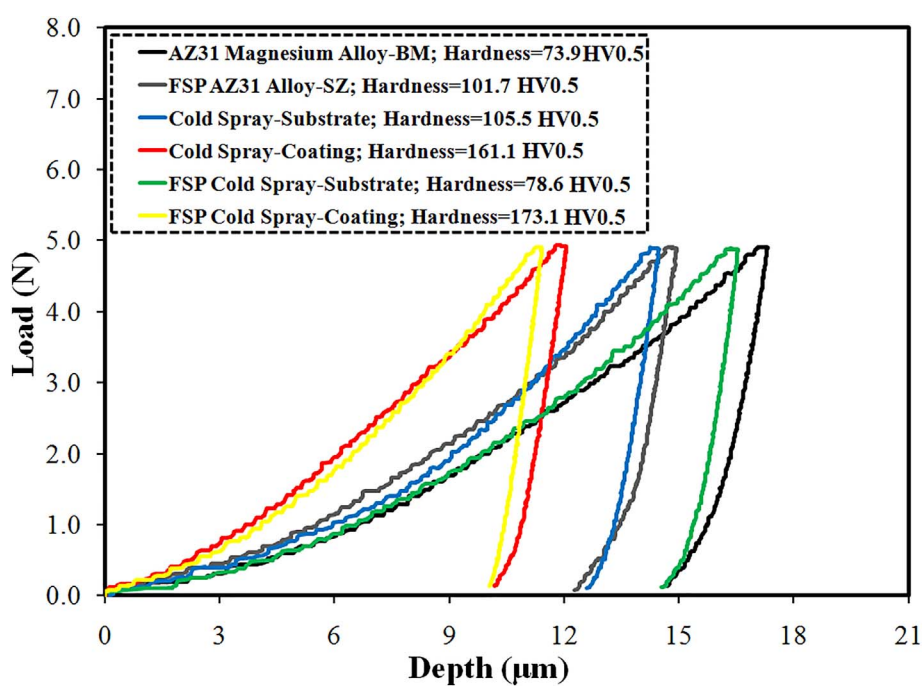


**Fig. 15.** Indentation load-displacement graphs and the related hardness values for the AZ31B alloy and cold sprayed AZ31B-AA7075 structure before and after FSP.

improved up to more than two times depending on the location and the AZ31B substrate tempering condition. This can be attributed to the higher hardness of AA7075 alloy in a T6 temper condition, and the very high strain rate severe plastic impingement action during the FSP process. After FSP modification of cold sprayed bi-metallic structure, the local mechanical properties vary depending on the temperature and strain fields during FSP process at different regions in relation to the microstructural features as displayed in Figs. 5 to 9. As shown in Fig. 14d, the hardness of the magnesium substrate under the cold sprayed layer after FSP is reduced due to the grain structural coarsening and annealing of dislocations. Meanwhile, the indentation hardness of the cold sprayed AA7075 layer is improved after FSP modification under the shoulder, owing to the structural densification and grain refinement. In comparison between the Fig. 14d–e, one can observe that the enhanced mechanical properties of the coating after employing FSP process are not uniform at different regions, and vary from advancing side toward the retreating side of the FSP process due to differences in the microstructural features.

In the middle regions close to the pin, the hardness improvement is lower than the regions close to the shoulder edge. Since the outer edge of the tool surface interface experiences higher shear strains, this will lead to intensified microstructure refinement. In the center region of the SZ, considerable hardness improvements with respect to the initial magnesium alloy are established, as shown in Fig. 14f, with a peak increase of ~150%. This can be deduced by the aluminum and magnesium alloys inter-mixing, grain structural refinement at the SZ, and the formation of inter-metallic secondary phase and ultra-fine reinforcing particles (see Fig. 8 and ESI Figs. S12). Therefore, a key finding of the present research employing FSP as a post-modification technique on a cold sprayed coating, the microstructures and mechanical performance of the deposited coating material can be considerably improved.

#### 4. Conclusions

In this research, cold gas dynamic spray deposition and friction-stir modification were applied as two complementary processes to produce a dense, homogenous, and hard coating metal layer (AA7075) on the surface of another metal substrate (AZ31B). It was found that the microstructure of substrate alloy refined close to the surface due to high temperature high velocity impingement during cold spraying process. Significant enhancement in the microstructural features and mechanical properties of the coating layer were achieved following FSP modification. Some grain coarsening under the shoulder and refinement around the small rotating pin were observed during the subsequent FSP modification, which leads to an improvement in Vickers hardness of the coating layer by more than three times as compared to the starting substrate alloy. Microstructures also indicate that the bonding mechanisms between the cold sprayed metal layer and substrate were reinforced significantly by the induced high temperature intense plastic deformation during FSP process, leading to improved material intermixing assisted by the elemental inter-diffusion and solid-state chemical reactions.

#### Appendix A. Supplementary data

Supplementary data to this article can be found online at <https://doi.org/10.1016/j.surfcot.2017.10.060>.

#### References

- [1] Y. Ali, D. Qiu, B. Jiang, F. Pan, M.X. Zhang, Current research progress in grain refinement of cast magnesium alloys: a review article, *J. Alloys Compd.* 619 (2015) 639–651.
- [2] J. Song, F. Pan, B. Jiang, A. Atrens, M.X. Zhang, Y. Lu, A review on hot tearing of magnesium alloys, *J. Magnesium and Alloys* 4 (2016) 151–172.
- [3] F. Pan, M. Yang, X. Chen, A. Review, On casting magnesium alloys: modification of commercial alloys and development of new alloys, *J. Mater. Sci. Technol.* 32 (2016) 1211–1221.
- [4] Y. Liu, H. Ren, W.C. Hu, D.J. Li, X.Q. Zeng, K.G. Wang, J. Lu, First-principles calculations of strengthening compounds in magnesium alloy: a general review, *J. Mater. Sci. Technol.* 32 (2016) 1222–1231.
- [5] E. Ghali, W. Dietzel, K.U. Kainer, General and localized corrosion of magnesium alloys: a critical review, *J. Mater. Eng. Perform.* 22 (2013) 2875–2891.
- [6] M. Asgari, M. Alioofkazraei, G.B. Darband, A.S. Rouhaghdam, Evaluation of alumina nanoparticles concentration and stirring rate on wear and corrosion behavior of nanocomposite PEO coating on AZ31 magnesium alloy, *Surf. Coat. Technol.* 309 (2017) 124–135.
- [7] Z. Száraz, Z. Trojanová, M. Zehetbauer, High-pressure torsion deformation of a magnesium-based nanocomposite, *Int. J. Mater. Res.* 100 (2009) 906–909.
- [8] M.F. Montemor, Corrosion Issues in Joining Lightweight Materials: A Review of the Latest Achievements, *Nanomaterials in Joining*, (2016), pp. 53–72.
- [9] J.E. Gray, B. Luan, Protective coatings on magnesium and its alloys — a critical review, *J. Alloys Compd.* 336 (2002) 88–113.
- [10] G.S. Cole, A.M. Sherman, Lightweight materials for automotive applications, *Mater. Charact.* 35 (1995) 3–9.
- [11] N. Bala, H. Singh, J. Karthikeyan, S. Prakash, Cold spray coating process for corrosion protection: a review, *Surf. Eng.* 30 (2014) 414–421.
- [12] S.M. Hassani-Gangaraj, A. Moridi, M. Guagliano, Critical review of corrosion protection by cold spray coatings, *Surf. Eng.* 31 (2015) 803–815.
- [13] H. Chang, M.Y. Zheng, C. Xu, G.D. Fan, H.G. Brokmeier, K. Wu, Microstructure and mechanical properties of the Mg/Al multilayer fabricated by accumulative roll bonding (ARB) at ambient temperature, *Mater. Sci. Eng. A* 543 (2012) 249–256.
- [14] H. Assadi, F. Gärtner, T. Stoltenhoff, H. Kreye, Bonding mechanism in cold gas spraying, *Acta Mater.* 51 (2003) 4379–4394.
- [15] X.T. Luo, C.X. Li, F.L. Shang, G.J. Yang, Y.Y. Wang, C.J. Li, High velocity impact induced microstructure evolution during deposition of cold spray coatings: a review, *Surf. Coat. Technol.* 254 (2014) 11–20.
- [16] M. Gruijicic, C. Zhao, C. Tong, W. DeRosset, D. Helfritch, Analysis of the impact velocity of powder particles in the cold-gas dynamic-spray process, *Mater. Sci. Eng. A* 368 (2004) 222–230.
- [17] S. Yin, M. Meyer, W. Li, H. Liao, R. Lupoi, Gas flow, particle acceleration, and heat transfer in cold spray: a review, *J. Therm. Spray Technol.* 25 (2016) 874–896.
- [18] H. Assadi, T. Schmidt, H. Richter, J.O. Kliemann, K. Binder, F. Gärtner, T. Klassen, H. Kreye, On parameter selection in cold spraying, *J. Therm. Spray Technol.* 20 (2011) 1161–1176.
- [19] M. Gruijicic, J.R. Saylor, D.E. Beasley, W.S. DeRosset, D. Helfritch, Computational analysis of the interfacial bonding between feed-powder particles and the substrate in the cold-gas dynamic-spray process, *Appl. Surf. Sci.* 219 (2003) 211–227.
- [20] M. Gruijicic, C.L. Zhao, W.S. DeRosset, D. Helfritch, Adiabatic shear instability based mechanism for particles/substrate bonding in the cold-gas dynamic-spray process, *Mater. Des.* 25 (2004) 681–688.
- [21] T. Schmidt, H. Assadi, F. Gärtner, H. Richter, T. Stoltenhoff, H. Kreye, T. Klassen, From particle acceleration to impact and bonding in cold spraying, *J. Therm. Spray Technol.* 18 (2009) 794.
- [22] S. Kumar, G. Bae, C. Lee, Influence of substrate roughness on bonding mechanism in cold spray, *Surf. Coat. Technol.* 304 (2016) 592–605.
- [23] A. Moridi, S.M. Hassani-Gangaraj, M. Guagliano, M. Dao, Cold spray coating: review of material systems and future perspectives, *Surf. Eng.* 30 (2014) 369–395.
- [24] Q. Wang, M.X. Zhang, Review on recent research and development of cold spray technologies, *Key Eng. Mater.* (2013) 1–52.
- [25] W. Li, K. Yang, D. Zhang, X. Zhou, X. Guo, Interface behavior of particles upon impacting during cold spraying of Cu/Ni/Al mixture, *Mater. Des.* 95 (2016) 237–246.
- [26] K. Spencer, D.M. Fabijanic, M.X. Zhang, The use of Al-Al<sub>2</sub>O<sub>3</sub> cold spray coatings to improve the surface properties of magnesium alloys, *Surf. Coat. Technol.* 204 (2009) 336–344.
- [27] B.S. DeForce, T.J. Eden, J.K. Potter, Cold spray Al-5% Mg coatings for the corrosion protection of magnesium alloys, *J. Therm. Spray Technol.* 20 (2011) 1352–1358.
- [28] D. Dzhrurinskiy, E. Maeva, E. Leshchinsky, R.G. Maeve, Corrosion protection of light alloys using low pressure cold spray, *J. Therm. Spray Technol.* 21 (2012) 304–313.
- [29] H. Bu, M. Yandouzi, C. Lu, D. MacDonald, B. Jodooin, Cold spray blended Al + Mg<sub>17</sub>Al<sub>12</sub> coating for corrosion protection of AZ91D magnesium alloy, *Surf. Coat. Technol.* 207 (2012) 155–162.
- [30] G. Shayegan, H. Mahmoudi, R. Ghelichi, J. Villafuerte, J. Wang, M. Guagliano, H. Jahed, Residual stress induced by cold spray coating of magnesium AZ31B extrusion, *Mater. Des.* 60 (2014) 72–84.
- [31] Q. Wang, N. Birbilis, M.X. Zhang, Process optimisation of cold spray Al coating on AZ91 alloy, *Surf. Eng.* 30 (2014) 323–328.
- [32] P. Cavaliere, A. Silvello, Processing conditions affecting residual stresses and fatigue properties of cold spray deposits, *Int. J. Adv. Manuf. Technol.* 81 (2015) 1857–1862.
- [33] F. Wang, Deposition characteristic of Al particles on Mg alloy micro-channel substrate by cold spray, *Int. J. Adv. Manuf. Technol.* (2016) 1–12.
- [34] M. Diab, X. Pang, H. Jahed, The effect of pure aluminum cold spray coating on corrosion and corrosion fatigue of magnesium (3% Al-1% Zn) extrusion, *Surf. Coat. Technol.* 309 (2017) 423–435.
- [35] W. Li, K. Yang, S. Yin, X. Yang, Y. Xu, R. Lupoi, Solid-state additive manufacturing and repairing by cold spraying: a review, *J. Mater. Sci. Technol.* (2017) Accepted Manuscript-In Press.
- [36] K. Yang, W.Y. Li, X.P. Guo, X.W. Yang, Y.X. Xu, Characterizations and anisotropy of cold-spraying additive-manufactured copper bulk, *J. Mater. Sci. Technol.* (2017) Accepted Manuscript-In Press.
- [37] I.S. Lee, C.J. Hsu, C.F. Chen, N.J. Ho, P.W. Kao, Particle-reinforced aluminum

- matrix composites produced from powder mixtures via friction stir processing, Compos. Sci. Technol. 71 (2011) 693–698.
- [38] R.S. Mishra, Z.Y. Ma, I. Charit, Friction stir processing: a novel technique for fabrication of surface composite, Mater. Sci. Eng. A 341 (2003) 307–310.
- [39] F.C. Liu, Z.Y. Ma, Contribution of grain boundary sliding in low-temperature superplasticity of ultrafine-grained aluminum alloys, Scr. Mater. 62 (2010) 125–128.
- [40] F. Khodabakhshi, H. Ghasemi Yazdabadi, A.H. Kokabi, A. Simchi, Friction stir welding of a P/M Al-Al<sub>2</sub>O<sub>3</sub> nanocomposite: microstructure and mechanical properties, Mater. Sci. Eng. A 585 (2013) 222–232.
- [41] H. Eskandari, R. Taheri, F. Khodabakhshi, Friction-stir processing of an AA8026-TiB<sub>2</sub>-Al<sub>2</sub>O<sub>3</sub> hybrid nanocomposite: microstructural developments and mechanical properties, Mater. Sci. Eng. A 660 (2016) 84–96.
- [42] F. Khodabakhshi, A.P. Gerlich, A. Simchi, A.H. Kokabi, Cryogenic friction-stir processing of ultrafine-grained Al-Mg-TiO<sub>2</sub> nanocomposites, Mater. Sci. Eng. A 620 (2015) 471–482.
- [43] F. Khodabakhshi, A. Simchi, A.H. Kokabi, M. Sadeghahmadi, A.P. Gerlich, Reactive friction stir processing of AA 5052-TiO<sub>2</sub> nanocomposite: process–microstructure–mechanical characteristics, Mater. Sci. Technol. 31 (2015) 426–435.
- [44] F. Khodabakhshi, A. Simchi, A.H. Kokabi, A.P. Gerlich, Friction stir processing of an aluminum-magnesium alloy with pre-placing elemental titanium powder: *In-situ* formation of an Al<sub>3</sub>Ti-reinforced nanocomposite and materials characterization, Mater. Charact. 108 (2015) 102–114.
- [45] R.S. Mishra, Z.Y. Ma, Friction stir welding and processing, Mater. Sci. Eng. R 50 (2005) 1–78.
- [46] B. Zahmatkesh, M.H. Enayati, A novel approach for development of surface nanocomposite by friction stir processing, Mater. Sci. Eng. A 527 (2010) 6734–6740.
- [47] P.B. Berbon, W.H. Bingel, R.S. Mishra, C.C. Bampton, M.W. Mahoney, Friction stir processing: a tool to homogenize nanocomposite aluminum alloys, Scr. Mater. 44 (2001) 61–66.
- [48] R. Nandan, T. DebRoy, H.K.D.H. Bhadeshia, Recent advances in friction-stir welding — process, weldment structure and properties, Prog. Mater. Sci. 53 (2008) 980–1023.
- [49] A. Simar, Y. Bréchet, B. de Meester, A. Denquin, C. Gallais, T. Pardoën, Integrated modeling of friction stir welding of 6xxx series Al alloys: process, microstructure and properties, Prog. Mater. Sci. 57 (2012) 95–183.
- [50] K.J. Hodder, H. Izadi, A.G. McDonald, A.P. Gerlich, Fabrication of aluminum–alumina metal matrix composites via cold gas dynamic spraying at low pressure followed by friction stir processing, Mater. Sci. Eng. A 556 (2012) 114–121.
- [51] C. Huang, W. Li, Y. Feng, Y. Xie, M.P. Planche, H. Liao, G. Montavon, Microstructural evolution and mechanical properties enhancement of a cold-sprayed CuZn alloy coating with friction stir processing, Mater. Charact. 125 (2017) 76–82.
- [52] H. Ashrafizadeh, A. Lopera-Valle, A. McDonald, A. Gerlich, Effect of friction-stir processing on the wear rate of WC-based MMC coatings deposited by low-pressure cold gas dynamic spraying, Proceedings Int. Therm. Spray Conference, 2015, pp. 41–47.
- [53] T. Peat, A. Galloway, A. Toumpis, P. McNutt, N. Iqbal, The erosion performance of cold spray deposited metal matrix composite coatings with subsequent friction stir processing, Appl. Surf. Sci. 396 (2017) 1635–1648.
- [54] C. Huang, W. Li, Z. Zhang, M.P. Planche, H. Liao, G. Montavon, Effect of tool rotation speed on microstructure and microhardness of friction-stir-processed cold-sprayed SiCp/Al5056 composite coating, J. Therm. Spray Technol. 25 (2016) 1357–1364.
- [55] C. Huang, W. Li, Z. Zhang, M. Fu, M.P. Planche, H. Liao, G. Montavon, Modification of a cold sprayed SiCp/Al5056 composite coating by friction stir processing, Surf. Coat. Technol. 296 (2016) 69–75.
- [56] P. Su, A. Gerlich, T. North, G. Bendzsak, Intermixing in dissimilar friction stir spot welds, Metall. Mater. Trans. A 38 (2007) 584–595.
- [57] Z.Y. Ma, Friction stir processing technology: a review, Metall. Mater. Trans. A 39 (2008) 642–658.
- [58] T.R. McNelley, S. Swaminathan, J.Q. Su, Recrystallization mechanisms during friction stir welding/processing of aluminum alloys, Scr. Mater. 58 (2008) 349–354.
- [59] T. Schmidt, F. Gärtner, H. Assadi, H. Kreye, Development of a generalized parameter window for cold spray deposition, Acta Mater. 54 (2006) 729–742.
- [60] A. Kurt, I. Uygur, E. Cete, Surface modification of aluminium by friction stir processing, J. Mater. Process. Technol. 211 (2011) 313–317.